ISSN 1027-5495. Functional Materials, 25, No.3 (2018), p. 490-495.
doi:https://doi.org/10.15407/fm25.03.490

Oxidation states and microstructure of manganese impurity centers in nanosized Al_2O_3 obtained by combustion method

***I.V.Berezovskaya*[1], *O.V.Khomenko*[1], *N.I.Poletaev*[2], *M.E.Khlebnikova*[2], *I.V.Stoyanova*[1], *N.P.Efryushina*[1], *V.P.Dotsenko*[1]**

[1]A.Bogatsky Physico-Chemical Institute, National Academy of Sciences of Ukraine, 86 Lustdorfskaya Doroga Str., 65080 Odessa, Ukraine
[2]Institute of Combustion and Advanced Technologies, Mechnikov Odessa National University, 2 Dvoryanskaya Str., 65082 Odessa, Ukraine

Received May 4, 2018

Nanosized (10–70 nm) Al_2O_3 doped with manganese ions (Mn^{3+}) was obtained by combustion method. It was found that the resulting powder consists of a mixture of transition aluminas (δ^*, δ, θ), among which δ^*-phase is dominant. It was shown that a part of Mn ions exists in the oxidation state +2 and occupies tetrahedral positions in δ^*–Al_2O_3, causing a broadband luminescence with a maximum at ~ 520 nm. Annealing in air at temperatures ≥1130°C results in the formation of stable α-polymorph. It is shown that the δ^*, $\theta \rightarrow \alpha$–$Al_2O_3$ phase transition is followed by oxidation of Mn^{2+}/Mn^{3+} ions and the stabilization of some amount of manganese ions in the oxidation state +4 on octahedral Al positions.
Keywords: nanoparticles, aluminum oxide, manganese, luminescence.

Наноразмерный (10–70 нм) Al_2O_3, активированный ионами марганца (Mn^{3+}), получен методом горения. Установлено, что конечный продукт представляет собой смесь метастабильных модификаций (δ^*, δ, θ) Al_2O_3, среди которых δ^*-фаза оказывается доминирующей. Показано, что часть ионов Mn находится в состоянии окисления +2 и занимает в δ^*–Al_2O_3 тетраэдрические позиции, обусловливая широкую полосу люминесценции с максимумом при ~520 нм. Обжиг на воздухе при температурах ≥1130°C приводит к формированию стабильной α-модификации Al_2O_3. Показано, что фазовый переход δ^*, $\theta \rightarrow \alpha$–$Al_2O_3$ сопровождается окислением Mn^{2+}/Mn^{3+}, и стабилизацией некоторой части ионов марганца в состоянии окисления +4 в октаэдрических позициях Al.

Стани окиснення та мікроструктура домішкових центрів мангану у нанорозмірному Al_2O_3, отриманому методом горіння. *І.В.Березовська, О.В.Хоменко, М.І.Полєтаєв, М.Є.Хлебникова, І.В.Стоянова, Н.П.Єфрюшина, В.П.Доценко.*

Шляхом газофазного горіння отримано нанорозмірний (10–70 нм) оксид алюмінію (Al_2O_3), активований іонами мангану (Mn^{3+}). Встановлено, що кінцевий продукт являє собою суміш метастабільних модифікацій (δ^*, δ, θ) оксиду алюмінію, серед яких δ^*-фаза є домінуючою. Показано, що частина іонів мангану знаходиться у стані окиснення +2, займає у структурі тетраедричні позиції та обумовлює широку смугу люмінесценції з максимумом при ~ 520 нм. Випал на повітрі при температурах ≥1130°C призводить до формування стабільної α-модифікації Al_2O_3. Показано, що фазовий перехід δ^*, $\theta \rightarrow \alpha$–$Al_2O_3$, супроводжується окисненням Mn^{2+}/Mn^{3+} та стабілізацією мангану у стані окиснення +4 в октаедричних позиціях Al.

1. Introduction

Aluminum oxide (Al_2O_3) exists in numerous polymorphs. Thermodynamically stable α-polymorph is one of the most important functional materials due its exceptional properties such as high hardness, chemical inertness and a very high melting temperature. It finds a variety of applications in micro- and optoelectronics, different technologies of composition materials. Because of fine particle size, large surface area ($0.5–1.5 \cdot 10^2$ m^2/g), the metastable polymorphs also have applications, e.g., as adsorbents, abrasives and components of different catalysts. In the structure of α–Al_2O_3, all the Al^{3+} ions are octahedrally coordinated, whereas in metastable polymorphs Al^{3+} ions occupy tetrahedral (Al_{tetr}) and octahedral (Al_{oct}) sites. According to [1], the crystal structures of the metastable polymorphs can be described as ordered or partially disordered Al atoms arrays on the interstitial sites of an approximately close-packed oxygen sublattice. The phase transitions between these polymorphs involve mainly the arrangement of aluminum ions on the interstitial sites of the oxygen sublattice.

The optical and luminescent properties of α–Al_2O_3 are mainly determined by oxygen vacancies in the form of various *F*-centers [2, 3]. Some of these defects were found to be present in nanostructured Al_2O_3 polymorphs [4–6], but no specific size effects were revealed. Comparison of the luminescence properties of microsized and nanostructured Al_2O_3 showed that the photoluminescence of nominally pure nanosized Al_2O_3 (δ, θ-polymorphs) is mainly caused by the presence of uncontrolled impurities of *d*-elements, namely Ti, Cr, Fe [7, 8].

Due to the polymorphism of Al_2O_3, the possibility of controlling the surface morphology of particles, composites of Al_2O_3 with manganese oxides are effective and thermally stable catalysts of various chemical processes [9]. In particular, nanosized composite Al_2O_3/Mn_3O_4 has been recently proposed as a promising catalyst for the photostimulated degradation of some organic toxins on the surface of adsorbents [10]. It is known that nanostructured materials have some advantages over their microsized analogues, especially in the field of different coating technologies and optoelectronics. Despite the use of manganese ions (Mn^{3+})-doped Al_2O_3 as a pink pigment for the production of color ceramics [11], information on the optical and luminescent properties of Mn^{3+}/Mn^{2+} ions in Al_2O_3 is limited by α-modification [12]. The purposes of this work were to obtain nanosized Al_2O_3 activated by manganese ions, and to analyze the microstructure of Mn impurity centers in synthesis products.

2. Experimental

Non-doped nanosized Al_2O_3 and Mn^{3+}-doped Al_2O_3 with nominal concentrations of Mn 0.1 at.% were obtained by a gas-dispersed synthesis (GDS). This method is based on the combustion of powdered metals due to exothermic oxidizing reactions between them and a gaseous oxidizer (typically O_2) [13]. As shown earlier, this synthesis approach provides a favorable morphology of Al_2O_3 particles and a good dispersibility of the final product in various mediums [13, 14], which creates the potential for the production of luminescent ceramic materials and films. The details of the synthesis method and experimental setup used in this study were described previously in [13]. To obtain Mn-doped Al_2O_3, the appropriate amount of $MnCl_2$ was dissolved in ethanol. Then, the resulting solution was gradually added, with thorough mixing, to an aluminum powder (ASD-4) with an average particle size of 4.8 μm. After drying in air at 50°C, the as-obtained mixture was dispersed in N_2 and injected through an inner tube into O_2 stream. After ignition by an external source (flame from a propane torch), a stable two-phase diffusion dust flame was observed. The condensed products of aluminum combustion were collected using a fabric filter.

The samples were analyzed in the as-prepared state and after annealing at 800, 1000, 1130 and 1300°C for 3 h in air. X-ray diffraction (XRD) studies were carried out on a Shimadzu LabX XRD-6000 automated diffractometer using Cu K_α radiation (λ = 1.5418 Å). XRD patterns were mainly obtained in step scan mode (2θ step 0.02°) at a count time of 8 s per point. The study of particles size distribution and their morphology was performed by means of transmission electron microscopy (TEM) on a Philips EM-400 microscope. The emission and excitation spectra in UV-visible region were recorded at room temperature and 77 K using a Fluorolog FL-3-22 (Horiba Jobin Yvon) spectrofluorometer equipped with a xenon lamp as an excitation source. The decay time measurements were performed on a phosphorimeter FL-1040 (Horiba Jobin Yvon). A xenon flash lamp

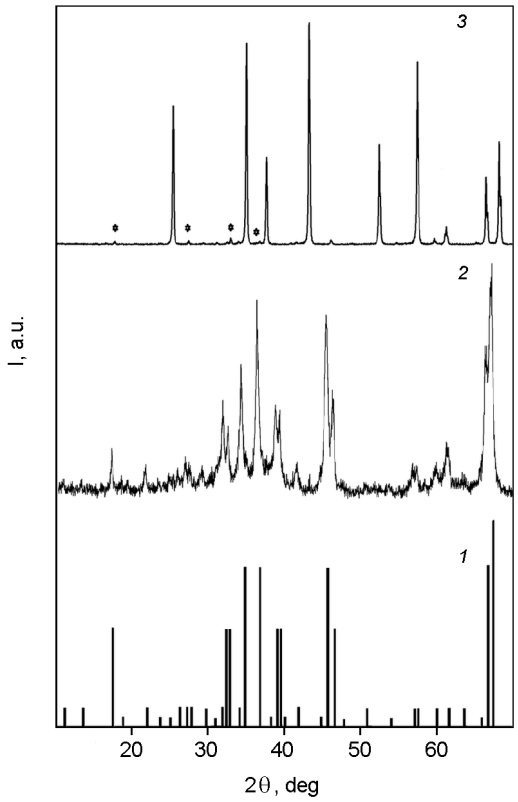

Fig. 1. Comparison of XRD pattern of the as-prepared $Al_2O_3:Mn^{3+}$ (*2*) with data from ICDD PDF-2 file No. 00-046-1215) for pure δ^*–Al_2O_3 (*1*); (*3*) — XRD pattern of $Al_2O_3:Mn^{3+}$ after annealing at 1300°C for 3 h in air. Peaks from θ–Al_2O_3 are denoted by the symbols (*).

with a pulse duration of ~ 4 μs was used in these measurements. Diffuse reflection spectra at room temperature were obtained on a spectrometer Perkin-Elmer Lambda 9.

3. Results and discussion

The XRD pattern of the as-prepared $Al_2O_3:Mn^{3+}$ is shown in Fig. 1. It appeared to be quite analogous to that of the non-doped sample (see, e.g., [14]). It should be noted that the diffraction peaks are sharp and narrow, suggesting a relatively high degree of crystallinity of the sample. From Fig. 1, it is seen that the main peaks match well with data from ICDD PDF-2 file No. 00-046-1215 for pure δ^*-polymorph of Al_2O_3. According to the XRD data, the samples consist of a mixture of transition aluminas (δ^*, δ, θ), among which δ^*-polymorph is dominant. Note that for high temperature gas-phase processes the formation of δ^*–Al_2O_3 is not exceptional phenomenon. This phase has been found to be dominant in Al_2O_3 powders obtained by a liquid-feed flame spray pyrolysis of metalloorganic precursors [15].

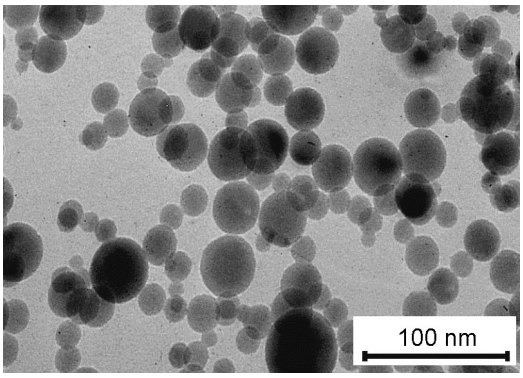

Fig. 2. TEM image of the as-prepared $Al_2O_3:Mn^{3+}$.

Earlier we showed that DTA curve of non-doped Al_2O_3 prepared by the GDS reveals a strong exothermic effect in the 1130–1400°C range with a maximum (T_{max}) at 1296°C, which is due to the θ → α–Al_2O_3 phase transition [16]. This phase transition was the subject of numerous studies, and at present it is known that α-Al_2O_3 is formed through a nucleation and growth process and depending on the chemical prehistory of the precursor, the degree of its crystallinity, the presence of impurities, etc. the T_{max} of this transition varies from 950 to 1350°C [1, 17, 18]. In full accordance with the DTA data [16], annealing at 800 and 1000°C did not lead to changes in the phase composition of the initial samples, while annealing at 1130°C was accompanied by an increase in the θ-phase content and the formation of some amounts of α–Al_2O_3. The X-ray diffraction pattern of the sample annealed at 1300°C for 3 h coincides with the literature data for α–Al_2O_3, although trace amounts (<2 %) of θ–Al_2O_3 were also detected (see Fig. 1).

TEM image of the as-prepared $Al_2O_3:Mn^{3+}$ is presented in Fig. 2. One can see that its particles are of spherical in shape with 10–70 nm in diameter, and no distinct manifestations of coalesce and agglomerate formation are observed. One can expect that the short time during which particles are exposed to high temperature and quick cooling to room temperature cause spherical form of the particles and limit their aggregation. Since the dust flame temperatures for Al-particles combustion (2600–2900°C) [13, 19, 20] are essentially higher than the θ → α-phase transition temperatures, one can expect that the phase composition and particle size distribu-

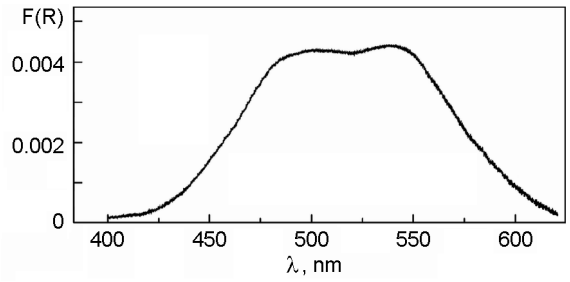

Fig. 3. Kubelka-Munk transformed diffuse reflection spectrum of the as-prepared $Al_2O_3:Mn^{3+}$.

tion of the materials obtained are mainly determined by kinetic factors. Note also that the XRD and electron microscopy data obtained in this study did not reveal any significant effect of Mn (for the concentration of $MnCl_2$ used) on the phase and grain-size compositions of the final product.

In contrast to non-doped sample, introduction of Mn into the Al_2O_3 lattice resulted in the formation of a pink colored sample. The diffuse reflection spectrum of the as-prepared $Al_2O_3:Mn^{3+}$ in visible region of spectrum is shown in Fig. 3. It can be seen that the spectrum consists of a wide absorption band in the 400–620 nm region with local maxima at ~ 490 and 537 nm. Note that the shape of absorption band, spectral position of its maxima are very similar to those for Mn^{3+}-doped α–Al_2O_3 [12, 21]. Analogous absorption spectra were also obtained for Mn^{3+}-doped yttrium aluminates $Y_3Al_5O_{12}$ [22] and $YAlO_3$ [23] and interpreted as a result of ${}^5E_g \rightarrow {}^5T_2$ transitions in Mn^{3+} ions at the octahedral Al_{oct} positions. A substantial half-width (~ 4000 cm^{-1}) of the Mn^{3+} absorption band in $Y_3Al_5O_{12}$ was attributed to Jahn-Teller splitting of both ${}^5E_g$ and ${}^5T_2$ states of Mn^{3+} [22]. Thus, the broad complex absorption band in the diffuse reflection spectrum of the as-prepared $Al_2O_3:Mn^{3+}$ is mainly due to the ${}^5E_g \rightarrow {}^5T_2$ transitions in Mn^{3+} ions occupying the octahedral Al_{oct} positions.

The emission spectra of non-doped δ^*–Al_2O_3 depend strongly on the excitation wavelength. At $\lambda_{exc} = 270$ nm, the spectrum consists of a band with a maximum at 450 nm and a shoulder at 412 nm. It was shown previously [16] that these features are caused by surface defects, the presence of which is quite typical for nanoscale inorganic materials. As can be seen from Fig. 4, the introduction of Mn ions leads to the appearance in the luminescence spectrum of a wide band in the region of 480–630 nm

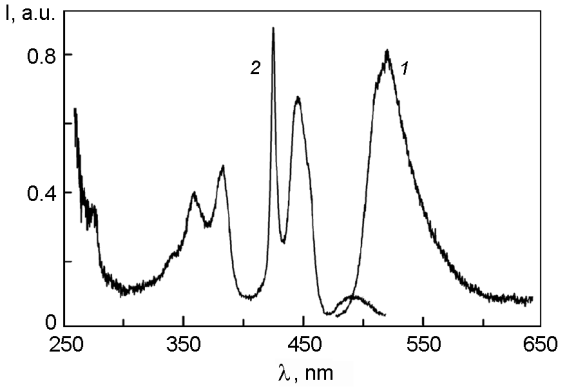

Fig. 4. Emission spectrum (*1*) at $\lambda_{exc} =$ 445 nm and excitation spectrum (*2*) of the as-prepared $Al_2O_3:Mn^{3+}$ ($\lambda_{em} = 520$ nm). The spectra were obtained at 293 K.

with a maximum at ~ 520 nm. It is evident that due to its spectral position this band cannot be associated with Mn^{3+} ions. One can suppose that this feature is due to the presence of Mn^{2+} ions, whose emission maximum position is strongly dependent on the crystal field strength at Mn^{2+} site.

Taking into account the literature data [24, 25] one can conclude that the luminescence with a maximum in the 510–530 nm range is typical for the ${}^4T_{1g}(G) \rightarrow {}^6A_{1g}({}^6S)$ transitions of tetracoordinated Mn^{2+} ions. This supposition agrees with the excitation spectrum for the emission band at 520 nm (see Fig. 4). According to the Tanabe-Sugano diagram for ions with $3d^5$ configuration (Mn^{2+}) [26], broad bands with maxima at 490 and 445 nm should be attributed to the ${}^6A_{1g}({}^6S) \rightarrow {}^4T_{1g}(G)$ and ${}^6A_{1g}({}^6S) \rightarrow {}^4T_{2g}(G)$ transitions, respectively. The relatively narrow and intense band at 425 nm, whose spectral position is characteristic for the tetracoordinated Mn^{2+} ion [24–26], is evidently caused by the ${}^6A_{1g}({}^6S) \rightarrow {}^4E_g$, ${}^4A_{1g}(G)$ transition. In the short-wavelength region of the spectrum there are bands at 342, 358 and 383 nm, which correspond to the ${}^6A_{1g}({}^6S) \rightarrow {}^4T_{1g}(P)$, ${}^6A_{1g}({}^6S) \rightarrow {}^4E_g(D)$ and ${}^6A_{1g}({}^6S) \rightarrow {}^4T_{2g}(D)$ transitions of Mn^{2+} ions. As can be seen from Fig. 3, the long-wavelength bands at ~ 490, 445 and 425 nm are absent in the diffuse reflection spectrum of the as-prepared sample. This can be explained by small oscillator strengths of the corresponding transitions from the ground level ${}^6A_{1g}$ of Mn^{2+} ions because these are spin- and parity-forbidden. Besides, one can expect that the concentration of Mn^{2+} ions in δ^*–Al_2O_3 is significantly lower than that of Mn^{3+}.

The decay of the luminescence emission at 510–530 nm was found to show a distinct deviation from the exponential behavior, and only in first approximation its main stage can be characterized by a time constant of $\tau = \sim 7.4$ ms. This value of decay time is close to those ($\tau = 4.8$–6 ms) reported in the literature for tetrahedrally coordinated ions Mn^{2+} in $ZnAl_2O_4$ [24], MgAlON [25]. The nonexponential character of luminescence decay for Mn^{2+} ions in δ^*–Al_2O_3 is probably due both to the structural disorder of metastable modifications and to local distortions of the symmetry of the Mn^{2+} centers located in proximity to the surface of the nanoparticles.

Thus, the as-prepared sample contains, in addition to Mn^{3+}, a part of Mn impurity ions in the oxidation state +2. It is clear that the Mn^{2+} content depends on the concentration of oxygen vacancies, which are a typical kind of intrinsic defects in various modifications of Al_2O_3. Their concentration in δ^*–Al_2O_3, obtained by the GDS method, is determined by a number of factors, including the partial pressure of O_2 in the reaction zone, the cooling rate of the combustion products, but it is expected to be relatively high, since one of the intermediate products of Al combustion is suboxide Al_2O_2 [19, 20].

The interpretation proposed above for the luminescence and diffuse reflection spectra of the as-prepared Al_2O_3:$Mn^{3+/2+}$ sample is supported by character of changes in these spectra caused by additional annealing in air for 3 h at 1130 and 1300°C. Note that annealing at 800 and 1000°C did not lead to any significant changes in the intensity and spectral composition of the emission, whereas the luminescence spectra of Al_2O_3:Mn^{3+} samples annealed at 1130 and 1300°C differed markedly from the spectrum of the as-prepared sample. In particular, in the luminescence spectra of the sample annealed at 1130°C, in addition to the band at 520 nm, there is an intense band in the 625–800 nm region with a maximum at 678 nm and a shoulder near 694 nm. There is no doubt about the nature of the band at 678 nm, because the identical spectrum was obtained earlier for Mn-doped α–Al_2O_3 [12, 27], and was interpreted as a result of the $^2E_g \rightarrow {}^4A_{2g}$ transition of Mn^{4+} ions. Therefore, the band at 678 nm should be attributed to Mn^{4+} ions in α-modification, the formation of which at 1130°C agrees with the XRD data. This conclusion does not contradict the emission and luminescence excitation spectra of the Al_2O_3:Mn^{3+} sample annealed at 1300°C (see Fig. 5). At room temperature, the emission spectrum contains an intense band at 678 nm with a long-wavelength tail extending up to 770 nm, which, as mentioned above, are due to the $^2E_g \rightarrow {}^4A_{2g}$ transition of Mn^{4+} ions and vibronic transitions, respectively. It is seen from Fig. 5 that at 77 K the emission spectrum exhibits a fine structure which corresponds to the above-mentioned interpretation of the room temperature spectrum. It consists of two relatively narrow bands at 672.9 and 676.4 nm, known as *R*-lines, and broader bands of lower intensity at 683–702 nm caused by the electron-phonon interaction in the Mn^{4+} impurity center of α–Al_2O_3 [12]. It is important to note that the spectra do not contain the luminescence band at 520 nm characteristic for the Mn^{2+} ions in δ^*–Al_2O_3, which confirms the absence of this modification in the sample annealed at 1300°C.

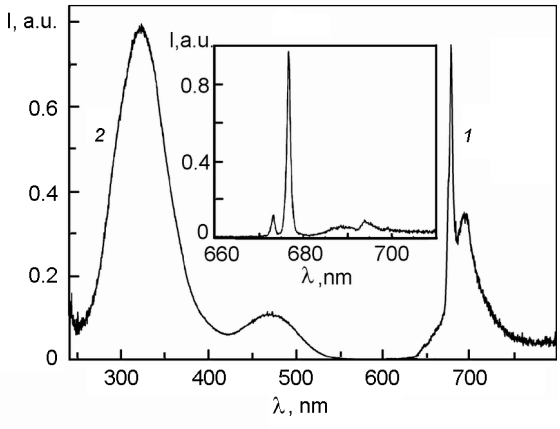

Fig. 5. Emission (*1*) and excitation (*2*) spectra of Al_2O_3:Mn^{3+} at 293 K after annealing at 1300°C in air. The inset shows the emission spectrum at 77 K. The emission spectra were recorded upon excitation at $\lambda_{exc} = 325$ nm.

It can also be seen from Fig. 5 that the excitation spectrum for the luminescence of Mn^{4+} ions in α–Al_2O_3 consists of a broad intense band with a maximum at 323 nm and a less intense one at 476 nm. The latter is obviously due to the $^4A_{2g} \rightarrow {}^4T_{2g}$ transition of Mn^{4+} ions, whereas interpretation of the former band is multi-valued. In [12], the band at 323 nm was attributed mainly to a charge-transfer transition from 2*p* orbitals of O atoms to the Mn^{4+} vacant orbitals. An analogous band at 317 nm was shown to be present in the luminescence excitation spectra for Mn^{4+} ions in $GdAlO_3$. Based on

the calculations for Mn^{4+} energy levels in $GdAlO_3$ in the framework of the exchange charge model of crystal-field theory, it was interpreted as a superposition of the $O^{2-} \rightarrow Mn^{4+}$ charge transfer band and a band due to the ${}^4A_{2g} \rightarrow {}^4T_{1g}$ transitions of Mn^{4+} ions located in Al_{oct} positions [28]. Note that the as-prepared sample and the products of its annealing at 800–1300°C did not show any luminescence that could be attributed to Mn^{3+} ions. This result agrees with the conclusion of the authors [12] about the absence of any luminescence from Mn^{3+} ions in α–Al_2O_3 even at 4.2 K.

Thus, in the present work, the possibility of doping Al_2O_3 with $Mn^{3+/2+}$ ions in the process of aluminum combustion in a gas-dispersion system is shown. Since the synthesis method allows its adaptation to obtain Al_2O_3 with Mn concentrations up to 1–2 at.%, and taking into account the favorable particle size distribution and high reactivity of the final product, one can suppose that nanosized Al_2O_3:$Mn^{3+/2+}$ can also be of interest as an effective precursor for producing transparent luminescent ceramics with composition MgAlON:Mn^{2+} recommended for use in high-power light emitting diode sources [25].

4. Conclusions

The possibility of doping Al_2O_3 with Mn^{3+} ions in the process of aluminum combustion in a dust flame was shown. The final product was found to consist of a mixture of transition aluminas (δ^*, δ, θ), among which the δ^*-phase is dominant. By the means of luminescent spectroscopy it was shown that some part of Mn impurity ions exists in the oxidation state +2 and occupies tetrahedral positions in the δ^*–Al_2O_3, causing a broad luminescence band with a maximum at 520 nm. Additional annealing in air at temperatures ≥1130°C results in the formation of stable α-modification and significant changes of the luminescent properties. It is shown that the δ^*, $\theta \rightarrow \alpha$–$Al_2O_3$ phase transition is followed by oxidation of Mn^{2+}/Mn^{3+} ions and the stabilization of some amount of manganese ions in the oxidation state +4 on octahedral Al positions.

It is expected that, because of the favorable particle size and high reactivity, the nanoscale Al_2O_3:$Mn^{3+/2+}$ obtained by the combustion method can also be of interest as an effective precursor for the production of a transparent luminescent ceramic with composition MgAlON:Mn^{2+}.

References

1. I.Levin, D.Brandon, *J.Am.Ceram.Soc.*, **81**, 1995 (1998).
2. B.D.J.Evans, *J.Nucl.Mater.*, **219**, 202 (1995).
3. S.Ikeda, T.Uchino, *J.Phys.Chem.C*, **118**, 4346 (2014).
4. S.V.Gorbunov, S.O.Cholakh, V.A.Pustovarov et al., *Phys.Stat.Sol.(c)*, **2**, 351 (2005).
5. M.Kirm, E.Feldbach, A.Kotlov et al., *Radiat.Meas.*, **45**, 618 (2010).
6. Z.Wang, C.Li, L.Liu, T-K.Sham, *J.Chem.Phys.*, **138**, 084706 (2013).
7. L.Trinkler, B.Berzina, D.Jakimovica et al., *Opt.Mater.*, **32**, 789 (2010).
8. L.Trinkler, B.Berzina, Z.Jevsjutina et al., *Opt.Mater.*, **34**, 1553 (2012).
9. O.A.Bulavchenko, T.N.Afanasenko, P.G.Tsyrul'nikov et al., *Kinet.Catal.*, **55**, 671 (2014).
10. S.A.B.Asif, S.B.Khan, A.M.Asiri, *Nanosc.Res.Lett.*, **10**, 355 (2015).
11. E.Lopez-Navarrete, A.Caballero, A.R.Gonzalez-Elpe, M.Ocana, *J.Eur.Ceram.Soc.*, **24**, 3057 (2004).
12. A.Van Die, W.F.van der Weg, A.C.H.I.Leenaers, G.Blasse, *Mat.Res.Bull.*, **22**, 781 (1987).
13. A.N.Zolotko, N.I.Poletaev, Ya.I.Vovchuk, *Comb.Expl.Shock Waves.*, **52**, 252 (2015).
14. V.P.Dotsenko, I.V.Berezovskaya, E.V.Zubar et al., *J.Alloys Compd.*, **550**, 159 (2013).
15. T.Hinklin, B.Toury, C.Gervais et al., *Chem.Mater.*, **16**, 21 (2004).
16. I.V.Berezovskaya, N.I.Poletaev, M.E.Khlebnikova et al., *Meth.Appl.Fluoresc.*, **4**, 034011 (2016).
17. P.-L.Chang, F.-S.Yen, K.-C.Cheng, H.-L.Wen, *Nano Lett.*, **1**, 253 (2001).
18. J.Gangwar, B.K.Gupta, S.K.Tripathi, A.K.Srivastava, *Nanoscale*, **32**, 13313 (2015).
19. Y.Huang, G.A.Risha, V.Yang, R.A.Yetter, *Comb.Flame*, **156**, 5 (2009).
20. N.I.Poletaev, A.V.Florko, *Comb.Expl.Shock Waves*, **43**, 414 (2007).
21. D.S.McClure, *J.Chem.Phys.*, **16**, 2757 (1962).
22. S.Kuck, S.Hartung, S.Hurling et al., *Phys.Rev.B*, **57**, 2203 (1998).
23. M.A.Noginov, G.B.Loutts, M.Warren, *J.Opt.Soc.Am.B.*, **16**, 475 (1999).
24. L.Cornu, M.Duttine, M.Gaudon, V.Jubera, *J.Mater.Chem.C.*, **2**, 9512 (2012).
25. K.Li, H.Wang, X.Liu et al., *J.Eur.Ceram.Soc.*, **37**, 4229 (2017).
26. A.B.P.Lever, Inorganic Electronic Spectroscopy, Elsevier Science Publishers B.V. Amsterdam (1984).
27. Yu.D.Ivakin, M.N.Danchevskaya, O.G.Ovchinnikova et al., *Supercit.Fluids: Theor.Pract.*, **3**, 11 (2008).
28. A.M.Srivastava, M.G.Brik, *Opt.Mater.*, **63**, 207 (2017).